18TH WORLD CONFERENCE ON EARTHQUAKE ENGINEERING
WCEE2024
MILAN

MILAN, ITALY
30TH JUNE - 5TH JULY 2024
www.wcee2024.it

USE OF PHYSICS-BASED SIMULATED EARTHQUAKE GROUND MOTIONS FOR ANALYSIS OF NEAR-FAULT BUILDINGS

M. Kenawy[1] & A. Pitarka[2]

[1] Oklahoma State University, Stillwater, USA, mkenawy@okstate.edu

[2] Lawrence Livermore National Laboratory, Livermore, USA

Abstract: *Physics-based earthquake simulations are rapidly finding applications in structural engineering, supplementing the available earthquake record databases, and creating unprecedented opportunities for site-specific seismic analysis of structures. Due to advances in understanding of earthquake fault rupture processes and high-performance computing, simulated earthquake records are becoming increasingly indistinguishable from real records. However, the use of synthetic ground motions in performance-based seismic design is in its infancy, and there is little guidance on how to select simulated records for nonlinear time-history analysis of structures such that the expected seismic demands are appropriately represented. Selecting earthquake records for evaluating the risks to near-fault structures is particularly challenging because (1) earthquake-induced ground shaking in the near-fault region is highly sensitive to the fault rupture characteristics, seismic wave propagation patterns, and site conditions, and (2) field recordings of such near-fault shaking are relatively sparse. In this study, the use of broadband physics-based three-dimensional earthquake simulations in performance assessment of near-fault building structures is investigated. We explore the use of a large database of simulated ground motions in representing the characteristics of near-fault ground shaking and the demands on low-rise and high-rise buildings, and evaluate their performance against real earthquake recordings and the predictions of empirical ground motion models. The study demonstrates the advantages of using simulated near-fault ground motions to supplement the limited database of recordings for large earthquakes and short distances, and highlights potential deficiencies in earthquake simulations and empirical ground motion models for near-fault hazard and structural risk assessment. The findings of the study provide guidance on using physics-based earthquake simulations in performance-based design of buildings in urban areas near active faults.*

1. Introduction

Selecting earthquake records for nonlinear time-history analysis of civil structures is a critical link between hazard and risk analysis in performance-based earthquake engineering. Substantial efforts have been made over the past two decades to improve the procedures of sampling earthquake records that represent the expected hazard at a given site from the available database of observational records (NEHRP Consultants Joint Venture 2011, Shahi and Baker 2011, Bradley 2012, Hayden et al. 2014, Tarbali et al. 2019, Zengin and Abrahamson 2021). The selection of ground motion records for the analysis of structures that are proximate to active faults is challenging for several reasons: (1) near-fault ground motion intensity is widely variable and sensitive to the patterns of seismic wave propagation, fault rupture, and site amplification, (2) near-fault ground motion may include unique damaging characteristics that are not typically seen in far-field records, such as strong velocity pulses induced by rupture directivity effects, and (3) recordings of ground shaking for large earthquakes at short distances from the fault are relatively sparse in the available database of records, and may be underrepresented in empirical ground motion prediction models (GMPEs). Researchers have

proposed several methods to improve the representation of near-fault ground shaking intensity in engineering analysis, which may be categorized as follows:

- Using sophisticated ground motion intensity measures (IMs) other than the frequently used spectral acceleration at the first-mode period of the structure (e.g., Luco and Cornell 2007), especially those which are correlated with the nonlinear behavior of structures
- Incorporating modifications to empirical ground motion models to account for the spectral shapes of near-fault records (e.g., Somerville et al. 1997)
- Improving the selection of ground motion records for the analysis of near-fault structures by explicitly selecting ground motion records with strong directivity pulses (e.g., Shahi and Baker 2011). This approach relies on empirical models that classify near-fault records in a binary fashion as pulse or non-pulse, based on the presence of one dominating pulse in the ground velocity trace (Shahi and Baker 2014a), and estimating the likelihood of encountering a pulse-type ground motion at a given location.

The latter approach has been broadly incorporated in the ASCE 7 seismic design standard in the U.S. through guidance on explicitly considering near-fault pulses in the selection of ground motion records for the time-history analysis of near-fault buildings (ASCE 2016). This approach has also recently been criticized because of its representation of a continuous phenomenon (the increasing intensity of near-fault ground shaking due to the effects of rupture directivity) using a binary classification criterion (pulse or non-pulse) (Tarbali et al. 2019). A recent study by the authors also argued that this binary classification may not be appropriate for representing the characteristics of near-fault ground motions recorded on soft soils because such records can be dominated by multiple large pulses due to the effects of both rupture directivity and site amplification (Kenawy et al. 2023). Although more holistic approaches for representing the characteristics of near-fault ground motion have been proposed (for example, using the Generalized Conditional Intensity Measure (GCIM) approach (Tarbali et al. 2019)), identifying and representing the intensity characteristics of near-fault ground shaking is an area of ongoing research.

Physics-based earthquake simulations are a promising resource for studying the properties of near-fault ground motion, because they are capable of representing the rupture properties, fault geometry, site conditions and physics of wave propagation in three-dimensional media. Three-dimensional physics-based fault rupture simulations have evolved rapidly in recent years, and were used to study the response of structures to some earthquake scenarios (Marafi et al. 2019, Kenawy et al. 2021), but they remain relatively underutilized in earthquake engineering applications. Such simulations have the potential to produce synthetic earthquake records that supplement the available database of observational records, especially for relatively large events and short distances. In addition, as earthquake simulations evolve in tandem with scientific understanding of fault rupture processes and high-performance computing tools, they may be used to improve the representation of the target seismic hazard at near-fault locations which may be underrepresented in empirical ground motion models. In this article, we assess the utility of a large database of simulated earthquake ground motions in both aforementioned circumstances. We explore the use of the simulated ground motions in representing the characteristics of near-fault ground shaking for the analysis of modern building structures, and examine their performance against real earthquake recordings and the predictions of empirical GMPEs.

2. Study design

Suites of ground motion records are selected for the analysis of two near-fault building structures in an earthquake scenario-based context. We use a scenario representative of a magnitude 7.0 shallow crustal event, and Joyner Boore (JB) distance parameters of 1 km and 5 km. The averaged shear wave velocity in the top 30 meters (V_{s30}) is arbitrarily selected as 380 m/s (which corresponds to the smallest V_{s30} in the simulated earthquake scenario). The GCIM framework (Bradley 2012) is used to conduct the ground motion selection experiments, and a detailed description of our selection criteria is presented in the following sections. Each selection experiment is defined by the following: (1) the target distance metric (either 1 or 5 km), (2) the source of the target hazard spectra (either based on the empirical GMPEs, or based on the simulated earthquake scenario for the specified distance and soil properties), (3) the horizontal ground motion component represented by the target hazard spectra (either a strike-normal (SN) or strike-parallel (SP) component), and (4) the database from which the records are selected for the analysis (either simulated or real ground motion records). The full study matrix is described in Table 1, where every row corresponds to two

different record selection experiments, for a total of 16 experiments. The selection experiments were conducted on the basis of individual ground motion components because we are interested in comparing the response of structures associated with either the SN or SP components. We use the selection experiments to assess the performance of the earthquake simulations in the following ways:

- We compare the acceleration response spectra associated with the target scenario predicted by the earthquake simulations against the spectra indicated by the GMPE for the same causal parameters. We examine the median, 16th percentile and 84th percentile spectra corresponding to RotD50, in addition to two perpendicular horizontal components (SN and SP). In addition, we compare the structural demands imposed on representative building structures by suites of simulated ground motions selected to represent the parameters of each target hazard.
- We holistically evaluate the characteristics of the near-fault simulated ground motions against those of real near-fault ground motions by comparing the structural demands imposed by suites of simulated and real ground motion records selected to represent the same target hazard parameters.

Table 1. Parameters associated with the ground motion selection experiments

Index	Distance (km)	Component	Hazard Target	Selected Records
1, 2	1.0	SN, SP	GMPE	Real
3, 4	1.0	SN, SP	GMPE	Simulated
5, 6	1.0	SN, SP	Simulated	Real
7, 8	1.0	SN, SP	Simulated	Simulated
9, 10	5.0	SN, SP	GMPE	Real
11, 12	5.0	SN, SP	GMPE	Simulated
13, 14	5.0	SN, SP	Simulated	Real
15, 16	5.0	SN, SP	Simulated	Simulated

1.1. GMPE target hazard spectra

The target GMPE hazard for a given set of causal parameters (magnitude, distance and V_{s30}) is based on weighting the following empirical models: ASK14 (Abrahamson et al. 2014), BSSA14 (Boore et al. 2014), CB14 (Campbell and Bozorgnia 2014) and CY14 (Chiou and Youngs 2014), each receiving a normalized weight of 0.25 in the calculation of the RotD50 acceleration response spectra (Boore 2010). The empirical model proposed by Shahi and Baker (2014b) was used to obtain the median SN and SP target acceleration response spectra from the median RotD50 spectrum.

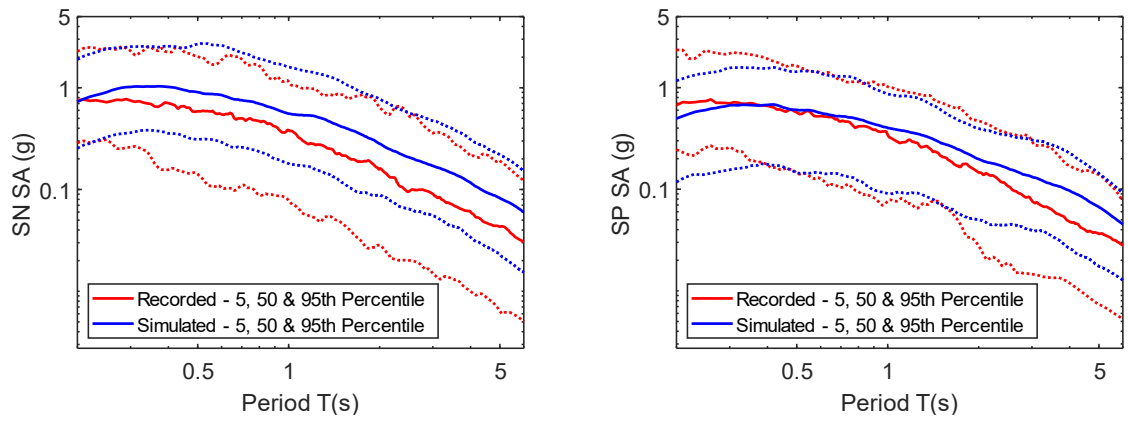

Figure 1. Median, 5th percentile and 95th percentile spectra of simulated and recorded (real) earthquake ground motions at distances less than or equal 15 km for the SN horizontal component (left) and SP horizontal component (right).

1.2. Simulation-based target hazard spectra

The statistical distribution of the spectral accelerations representing the simulation-based target hazard scenario were estimated directly from the simulated ground motions for the specified magnitude, distance and V_{s30} values. The target distribution should ideally incorporate the anticipated variability due to source, path and site effects. Our database represents some of the variability associated with the hypocenter location and rupture slip distribution, but is not comprehensive of all possible conditions. The RotD50 component of the simulated target hazard spectra was calculated based on the RotD50 definition in Boore (2010).

3. Database of recorded ground motions

The dataset of real near-fault ground motions is obtained from the PEER NGA-West2 database (Ancheta et al. 2014). It consists of 94 records, which were obtained by filtering the database for the following parameters: earthquake magnitudes between 6.7 and 7.4; JB distance between 0 and 15 km, and V_{s30} between 200 and 700 m/s. The range of magnitudes was selected such that the resulting records have a mean magnitude of 6.95, as close to the M7.0 simulated scenario as reasonably possible. The NGA-West2 records used in this study are listed in Appendix 1 in Kenawy et al. (2023). The as-recorded horizontal component accelerations were rotated to their SN and SP orientations based on the fault orientations extracted from the database.

4. Database of simulated ground motions

We use nine fully deterministic broadband (0-5 Hz) physics-based three-dimensional fault rupture realizations representing a M7.0 strike-slip earthquake scenario, which were generated using the finite difference code SW4 developed at Lawrence Livermore National Laboratory (LLNL) (Sjögreen and Petersson 2012). Six of these realizations were generated under the U.S. Department of Energy Exascale Computing Project (McCallen et al. 2021a) and three realizations were generated at LLNL using the Quartz computer. The kinematic earthquake rupture modeling technique of Graves and Pitarka was used to simulate the fault rupture processes (Graves and Pitarka 2016), which has been validated in simulations of recorded earthquakes (Pitarka et al. 2020, Pitarka et al. 2022). The rupture realizations represent common shallow crustal earthquakes with a predominantly strike-slip mechanism, and have different combinations of the hypocenter location, slip distribution characteristics, depth to the top of the rupture, and soil conditions, to capture some

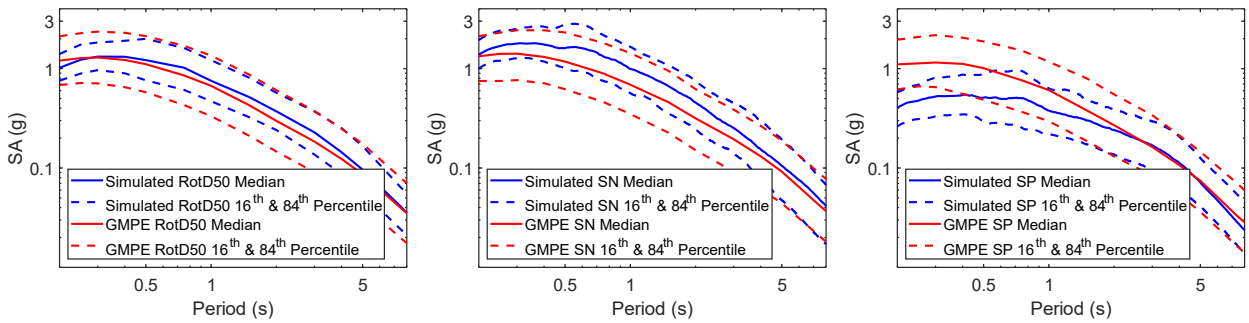

Figure 2. Target hazard spectra at a distance of 1 km based on simulated ground motions and GMPEs: RotD50 component (left), SN component (center), and SP component (right).

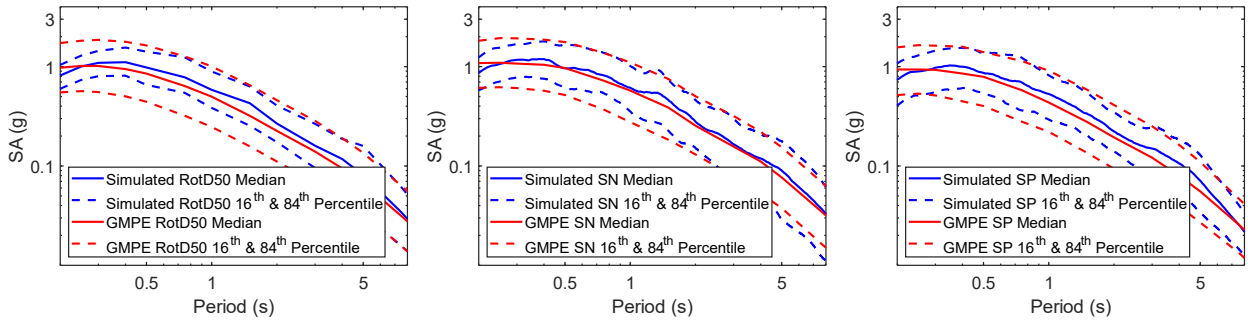

Figure 3. Target hazard spectra at a distance of 5 km based on simulated ground motions and GMPEs: RotD50 component (left), SN component (center), and SP component (right).

of the randomness associated with those parameters for a M7.0 scenario. An idealized velocity structure is used in the simulations to broadly represent relatively stiff and soft soils with a minimum shear wave velocity of 320 m/s. Further details about the rupture models, the computational domain and the velocity structure are provided in Kenawy et al. (2023) and Kenawy (2023).

The database of simulated ground motions consists of 35,640 horizontal records (where each record includes a SN and SP component) within a 20 km JB distance from the fault. The simulated ground motions are intended to produce records that are generally representative of shallow crustal earthquakes, but do not represent a specific historical event. The characteristics of a subset of this database were extensively studied and compared against those of real near-fault ground motion observations in Kenawy et al. (2023), revealing that the underlying idealized rupture model and velocity structure can represent the salient characteristics of near-fault observations. Of relevance to this study is the consistency between the spectral characteristics of the simulated and real ground motions, which is illustrated in Figure 1 for both the SN and SP components. The figure shows the median, 5th percentile and 95th percentile spectra associated with a near-fault subset of the simulated ground motions along with the NGA-West2 dataset of recordings. The NGA-West2 dataset includes records from earthquakes around the world with varying rupture mechanisms. Therefore, those records have a wider variability than the simulated ground motions, which is evidenced by the spread of the 5th and 95th percentile spectra of Figure 1 around the median spectrum. The median spectrum of the SN component of the simulated ground motions is consistently higher than that of the recorded ground motions, but the 95th percentile spectra of the two datasets are in reasonable agreement. The notable difference between the 5th percentile spectra of both datasets suggests that the ground motion simulations estimate somewhat higher shaking intensities compared with the near-fault real records, especially in the SN component. In contrast, the 5th, 50th, and 95th percentile SP acceleration spectra of the simulated ground motions appear to be consistent with those of the recorded ground motions across a broad range of periods. Above a period of 2 seconds, the median and 5th percentile SP spectra of the simulations are notably higher than those of the field recordings. However, for very short periods (between 0.2 and 0.3 s in this case), the spectral accelerations of the SP simulated ground motions tend to be smaller than those of the recorded ground motions. Overall, the trends reflect the consistency between the spectral characteristics of the simulated and recorded ground motions. In addition to the spectral shapes, the distance scaling of spectral accelerations and ground velocity, significant durations, velocity pulse features, and dominant pulse periods of the simulated ground motions were shown to be reasonably consistent with those of the recorded ground motions (Kenawy et al. 2023).

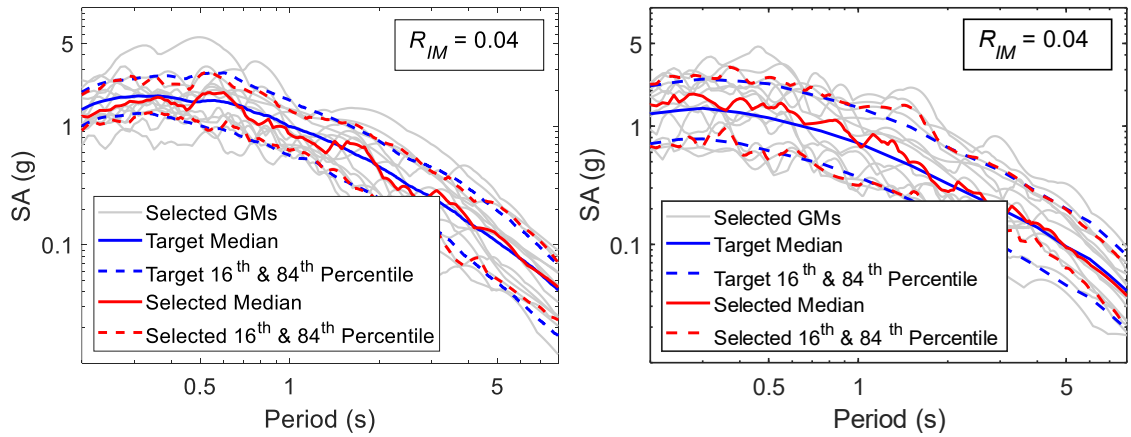

Figure 4. Selected ground motions representing SN simulated target spectra (left) and GMPE target spectra (right) for R = 1 km.

5. Structural analysis models

We use two reinforced concrete (RC) special moment frame buildings which were designed for seismic design category E: a 3-story building, and a 20-story building, following the seismic provisions of ASCE 7-16 (2016)

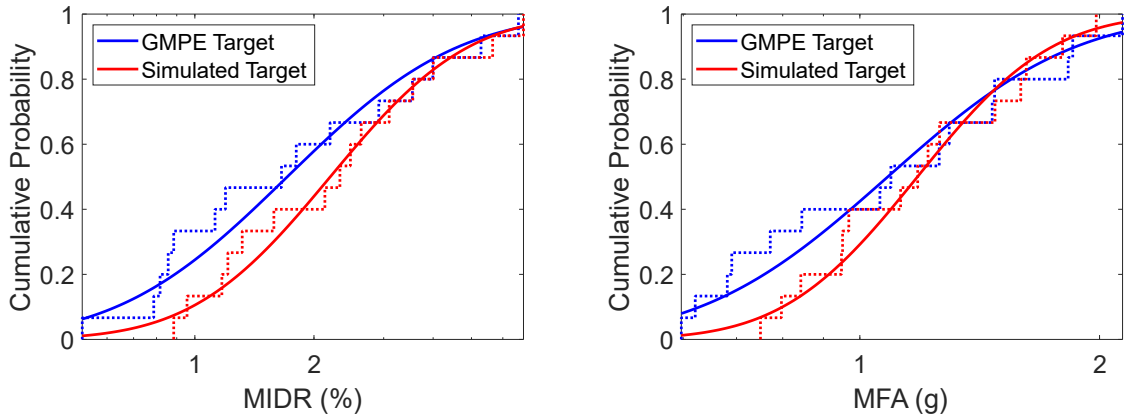

Figure 5. Empirical and fitted cumulative distributions of the MIDR (left) and MFA (right) demands imposed on the 3-story building by ground motions selected to represent SN GMPE and simulated target spectra at R = 1 km.

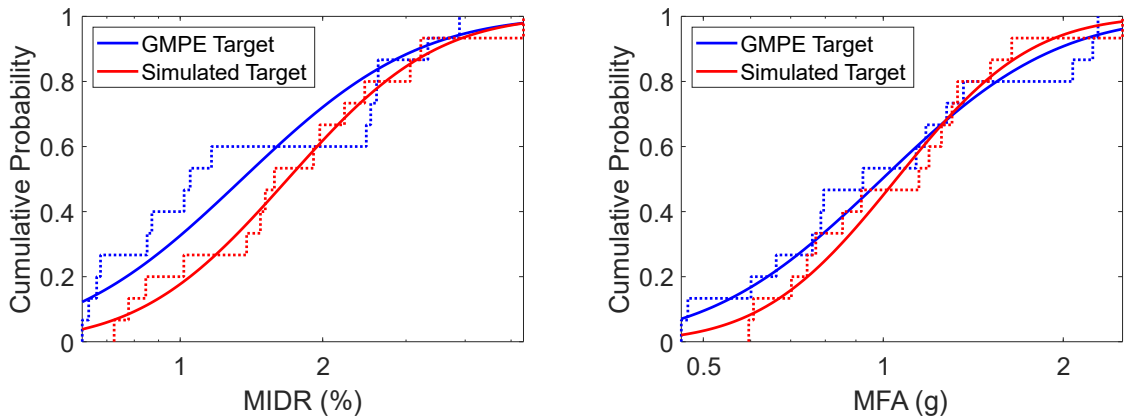

Figure 6. Empirical and fitted cumulative distributions of the MIDR (left) and MFA (right) demands imposed on the 20-story building by ground motions selected to represent SN GMPE and simulated target spectra at R = 1 km.

and the RC provisions in ACI 318-14 (2014). The seismic design is based on the risk-targeted maps for a site that is approximately two kilometers away from the Hayward fault in Berkeley, California with site class C. The first-mode period of the 3-story and 20-story buildings are 0.75 s and 3.45 s, respectively. Two-dimensional structural simulation models of representative building frames were created using the structural analysis platform Opensees (McKenna et al. 2000) using the lumped plasticity modeling approach (Giberson 1967). Further details about the structural design approach and simulation parameters are available in Kenawy et al. (2021) and Kenawy and McCallen (2021). Each building is subjected to the records selected based on the experiments described in Table 1, and the histories of the building interstory drifts and floor accelerations are recorded. In the following, we focus on the distributions of the maximum interstory drifts (MIDR) and maximum floor accelerations (MFA) as the structural demand parameters of interest.

6. Ground motion selection procedure

The ground motion selection experiments were conducted using the GCIM approach developed by Bradley (2012), which allows for holistic selection of ground motion records using the best fit to a vector of ground motion IMs. Details of the GCIM approach in a scenario-based context are described elsewhere (Tarbali and Bradley 2015), but the specific components of our selection method are summarized as follows:

- The target IMs consist of 20 spectral accelerations corresponding to the following periods: 0.01, 0.02, 0.03, 0.05, 0.075, 0.1, 0.15, 0.2, 0.25, 0.3, 0.4, 0.5, 0.75, 1, 1.5, 2, 3, 4, 5 and 6 seconds. We assign equal weights w_i to each spectral ordinate in the selection procedure.
- We draw random samples from the target IM distributions. For the simulation-based target spectra, the target IM sample consists of simulated ground motions drawn randomly and independently from the simulated records which constitute the target. Therefore, the correlations between the IMs (SAs at different periods) are inherently incorporated in the selection process. For the GMPE-based target spectra, random

realizations representing the multivariate distribution of the IMs are drawn using the approach described in Wang (2011), and the spectral acceleration correlations presented in Baker and Jayaram (2008).

- We evaluate the ground motion candidates against the target distribution sample using the square of the error between each target point and all the available candidate points. We assess the goodness of fit between the target IM distributions, and the distributions associated with the selected records using the Kolmogorov–Smirnov (K-S) test. A weighted measure of the goodness of fit of all the target IMs is calculated, following the recommendation of Bradley (2012) using the weights w_i and the square of the K-S test statistic D_{IM} as follows: $R_{IM} = \sum_{i=1}^{n} w_i D_{IM_i}^2$.

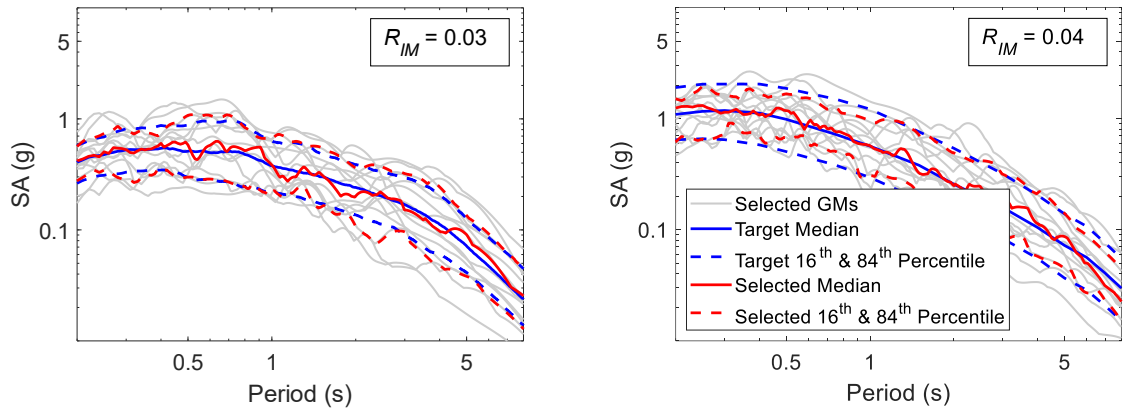

Figure 7. Selected ground motions representing SP simulated target spectra (left) and GMPE target spectra (right) at R = 1 km.

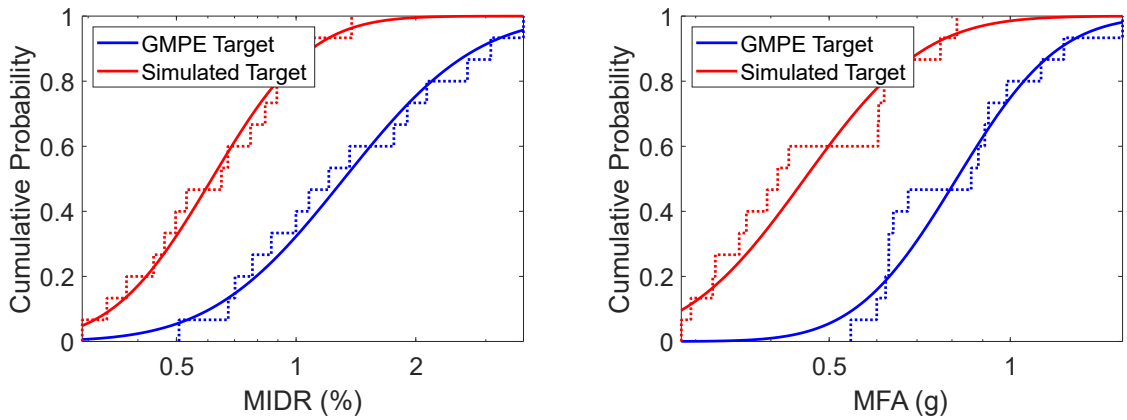

Figure 8. Empirical and fitted cumulative distributions of the MIDR (left) and MFA (right) demands imposed on the 3-story building by ground motions selected to represent SP GMPE and simulated target spectra at R = 1 km.

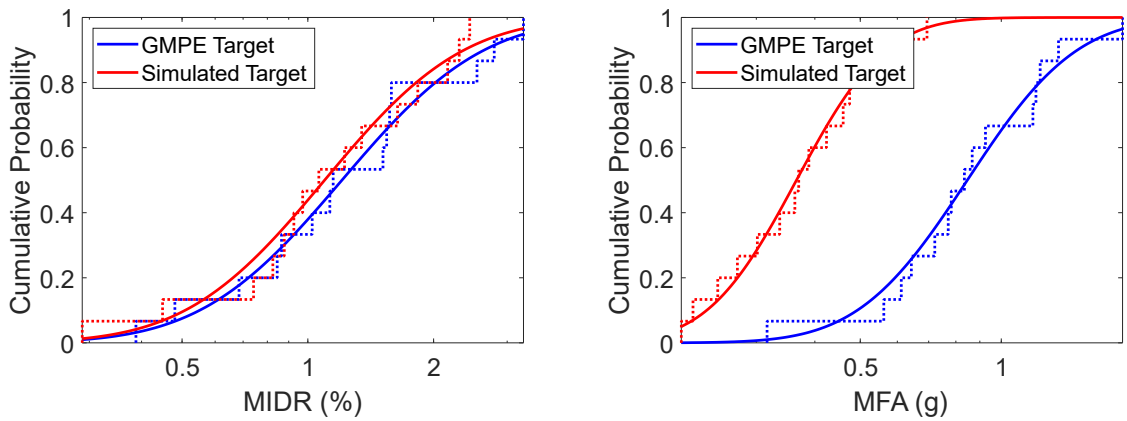

Figure 9. Empirical and fitted cumulative distributions of the MIDR (left) and MFA (right) demands imposed on the 20-story building by ground motions selected to represent SP GMPE and simulated target spectra at R = 1 km.

- We repeat this sampling process 15 times and select the best-fit ensemble of 15 ground motion records which yields the lowest global residual R_{IM}.

In this study, we did not need to perform scaling of the ground motion records to obtain an appropriate match to the target hazard, because the causal parameters of the record database are broadly similar to those of the target. However, a more comprehensive study may consider scaling of ground motion records from a broader database, which is a typical practice in earthquake engineering design procedures.

7. Results and discussion

7.1. Comparison between the simulated and GMPE ground motion target hazard spectra

Figure 2 shows the median, 16th percentile and 84th percentile target hazard spectra for a scenario with M = 7.0 and R = 1 km based on the simulated records for this scenario, plotted against the analogous GMPE-based spectra for the same causal parameters. The RotD50 spectra in the left subplot exhibit reasonable agreement between the simulation-based and GMPE-based spectra across a broad range of periods. Specifically, we compare the spectra across periods between 0.2 seconds (the lower limit represented by the earthquake simulations) and 8 seconds. Because the simulated records represent a small number of realizations, their spectra expectedly have narrower variability than the GMPE target spectra; therefore, the 16th percentile spectrum of the simulation-based target is notably higher than the 16th percentile spectrum of the GMPE target across most periods.

The individual horizontal component simulation-based spectra, however, differ more substantially from the estimated GMPE target spectra for the SN and SP components: Figure 2 reveals that the simulated SN component target median and 16th percentile spectra are higher than the GMPE target in the short- to mid-period range, whereas the 84th percentile spectrum of both targets appears to be similar across all periods. These trends are consistent with the trends observed when comparing the database of SN simulated near-fault ground motions against the real SN records, as discussed previously. On the other hand, the simulated SP target spectral accelerations are substantially smaller than the GMPE target spectral accelerations for periods up to approximately 2 seconds, as Figure 2 reveals. This observation is not consistent with the trends observed when comparing the simulated and real SP near-fault records shown in Figure 1, and the distance scaling trends noted in Kenawy et al. (2023). There are several potential reasons for this apparent inconsistency. First, because of the very small number of recorded ground motions for distances less than 5 km, the ground motion intensity at such short distances may be poorly represented by the empirical GMPEs. Second, the simulated ground motions, which represent a pure strike-slip mechanism with a vertical fault, may be highly polarized at very short distances, leading to larger SN and smaller SP spectral accelerations, compared with the general trends observed across the various fault geometries and rupture mechanisms employed in constructing the GMPEs. Examining the analogous target spectra at a distance of 5 km in Figure 3 demonstrates the consistency between the RotD50, SN and SP simulation-based and GMPE-based target hazard spectra, especially with respect to the median and 84th percentile spectra.

7.2. Structural demands imposed by records representing the GMPE and simulation-based spectra

The differences between the simulation-based and GMPE-based target hazard spectra are further highlighted in the context of their influence on the demands imposed on building structures with different dynamic characteristics. Figure 4 shows the results of record selection experiments from the database of simulated records, where the subplot on the left shows the results of using the SN simulated target hazard spectra, and the subplot on the right represents the analogous results using the SN GMPE target spectra. The global residual measure R_{IM} is shown in each subplot and is almost identical for both experiments. Figures 5 and 6 show the cumulative distributions of the structural demands corresponding to the selected suites of records in both cases on the 3-story and 20-story buildings, respectively. Empirical cumulative distributions for both the MIDR and MFA are plotted for each building, along with fitted lognormal distributions. As expected, the demands imposed by the records representing the simulated SN target spectra are higher than those imposed by the records representing the target GMPE SN spectra for both buildings. However, the differences between the demands imposed by each suite of records are not significant, based on the Mann-Whitney U (MWU) statistical test which assesses whether there is enough evidence in the data to reject the null hypothesis that both samples come from distributions with equal medians. The null hypothesis is not rejected in this case at a

significance level of 0.05 for the MIDR and MFA sample pairs for each building (p-values between 0.26 and 0.56 for the 3-story building, and between 0.38 and 0.53 for the 20-story building).

Substantially larger differences are observed between the structural demands predicted by representing the SP simulated or GMPE target hazard spectra (Figure 7). This is particularly the case for the demand parameters controlled by the high-frequency content of the ground motion records, such as the demands on the 3-story building, and the acceleration-based demand parameter (i.e., the MFA). These trends are shown in Figures 8 and 9 for the 3-story and 20-story, respectively. Much lower demands on the 3-story building are predicted by using a simulated hazard target, compared to a GMPE target. In the case of the 20-story building, the cumulative distribution of the displacement-based MIDR demands predicted in both cases is not significantly different, based on the MWU test (p-value = 0.87). However, the cumulative distributions of the MFA demands are significantly different based on the same test (p-value = 0.0001).

In agreement with the trends observed in Figure 3, most of the differences between the demands imposed by suites of records representing a simulated or GMPE-based target spectra diminish for both structures at a distance of 5 km. Specifically, the cumulative distributions of the MIDR and MFA demands imposed on the 3-story and 20-story buildings in both cases are not significantly different based on the MWU test (p-values between 0.25 and 0.93). These distributions are not shown here for brevity.

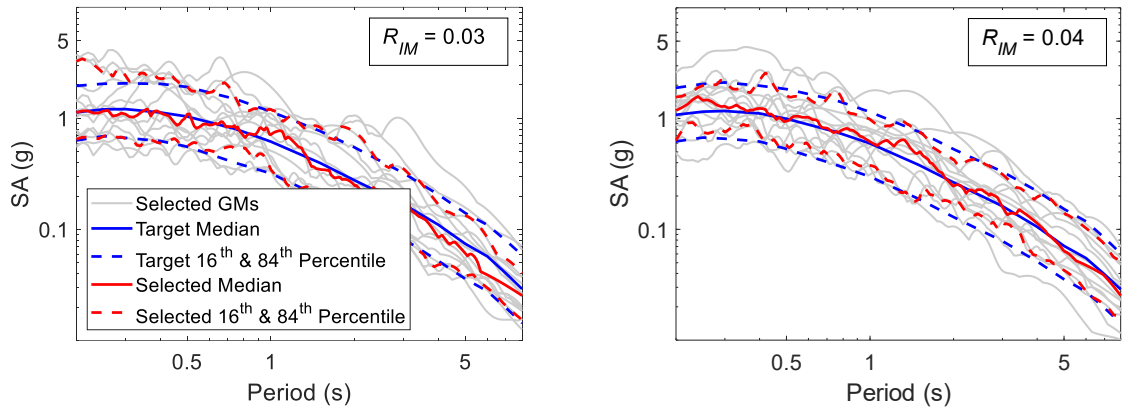

Figure 10. Selected real (left) and simulated (right) ground motions representing SP GMPE target spectra for R = 1 km.

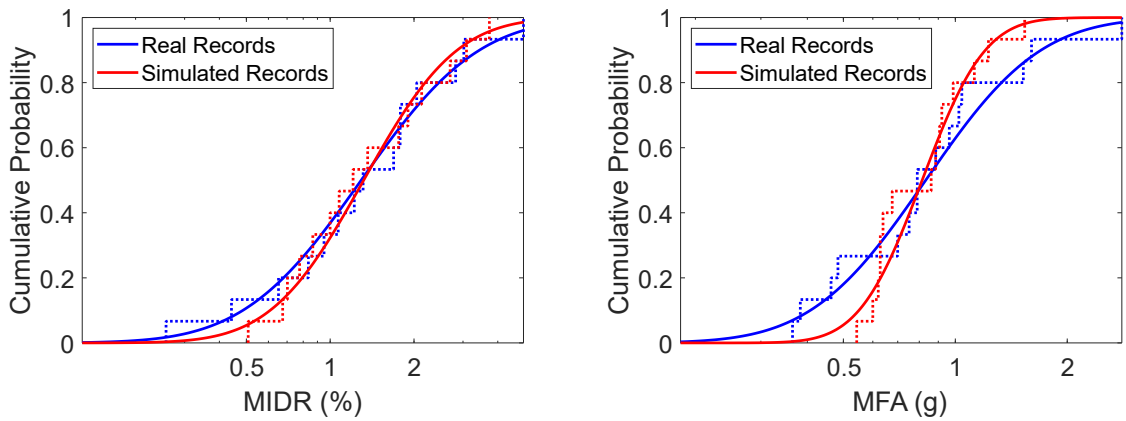

Figure 11. Empirical and fitted cumulative distributions of the MIDR (left) and MFA (right) demands imposed on the 3-story building by real and simulated ground motions selected to represent SP GMPE target spectra at R = 1 km.

7.3. Characteristics of simulated and real ground motions representing the same target hazard

In addition to assessing the potential for using simulated earthquake scenarios to represent the target hazard spectra in seismic risk analysis, we also test using simulated earthquake ground motions instead of, or in supplement to, real ground motions in the analysis of structures, after the target hazard parameters have been established. Simulated ground motions are useful in cases where there are not sufficient real records in the available observational databases with the desired characteristics (for example, records which correspond to distances shorter than 10 km and relatively large magnitude events). Figure 10 shows suites of ground motions selected to represent a target hazard based on the SP GMPE spectra at a distance of 1 km. The subplot on

the left shows the median, 16th percentile, and 84th percentile spectra of the selected records from the database of real near-fault ground motions, whereas the subplot on the right represents records selected from the database of simulated ground motions. It is noted that both selection experiments have a very similar global residual (noted in each subplot); i.e., the distributions associated with both suites of selected ground motions appropriately represent those associated the target spectra.

The structural demands corresponding to both suites of simulated and real records imposed on the 3-story and 20-story buildings are displayed in Figures 11 and 12, respectively. The plots demonstrate the consistency between the cumulative MIDR and MFA distributions imposed by the simulated and real ground motions, with no evidence of a statistically significant difference between each pair (two-sample MWU test, p-values between 0.9 and 1.0). More notable differences are observed between the demands imposed by the SN component of simulated and real records (compared to the SP component) but are not discussed here for brevity. Nonetheless, the results suggest that the simulated SN ground motions may tend to overestimate the structural demands in the short-period range (e.g., the demands on the 3-story building) and underestimate the demands in the long-period range (e.g., the MIDR demands on the 20-story building) compared to real SN ground motions selected to represent the same target hazard parameters.

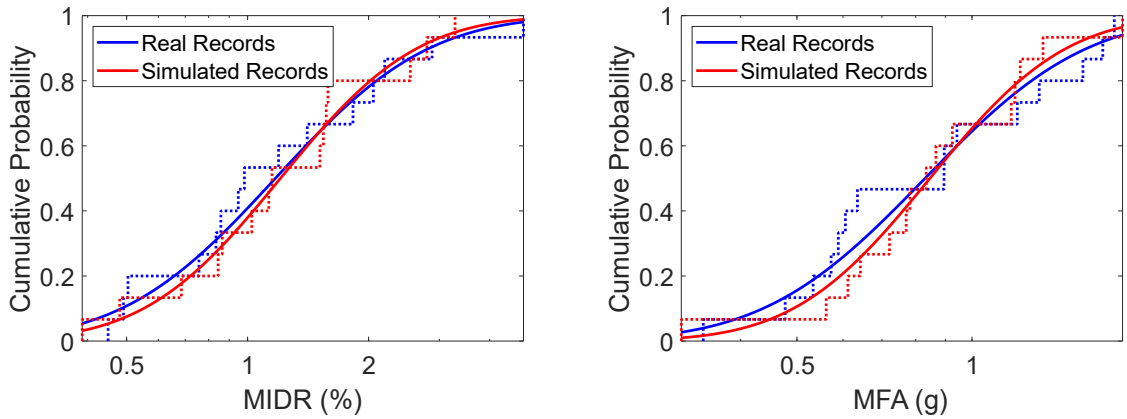

Figure 12. Empirical and fitted cumulative distributions of the MIDR (left) and MFA (right) demands imposed on the 20-story building by real and simulated ground motions selected to represent SP GMPE target spectra at R = 1 km.

8. Conclusions

In this study, we conduct ground motion record selection experiments to investigate the utility of physics-based earthquake simulations in the following contexts: (1) representing scenario-based target hazard parameters, and (2) supplementing or replacing real ground motion records when the latter are sparse for the causal parameters of interest. Our experiments show that the spectral shape features of the simulated earthquake scenario are broadly consistent with the GMPE target hazard spectra. However, a substantial difference between both sets of spectra is specifically noted in the SP component at the very short distance of 1 km. This difference may arise from conservatism built into the empirical models due to the lack of recorded ground motions at very short distances, but also signals the need for incorporating more variability into simulated earthquake scenarios before they can be used to represent target seismic hazard parameters at very short distances. The differences between the target hazard spectra propagate to the structural demands imposed by suites of records selected to represent either target, leading to significantly different demands in the short-period range. At the relatively larger near-fault distance of 5 km, most of the differences between the GMPE-based and simulation-based target spectra diminish, such that using the simulated earthquake scenario to represent the target hazard parameters could be expected to lead to appropriate earthquake records for engineering analysis.

After the target hazard parameters have been established, our analysis suggests that selected suites of real and simulated near-fault ground motions perform comparably, especially with regards to imposing similar demands on structures with varying dynamic characteristics. Keeping in mind the limited scope of the experiments performed in this study, these results support the use of broadband physics-based earthquake ground motions in engineering analysis of near-fault structures as a supplement to real earthquake records. Future extension of this work will compare the characteristics and impacts of simulated and real ground

motions for a wider range of distances and soil characteristics, and will incorporate additional randomness into the simulated rupture characteristics of shallow crustal earthquakes.

9. Acknowledgements

This material is based upon work supported by the U.S. Geological Survey under Grant No. G22AP00380. The views and conclusions contained in this document are those of the authors and should not be interpreted as representing the opinions or policies of the U.S. Geological Survey. Mention of trade names or commercial products does not constitute their endorsement by the U.S. Geological Survey. Arben Pitarka's work was performed under the auspices of the U.S. Department of Energy by LLNL under Contract Number DE-AC52-07NA27344. A portion of the ground motion simulations was performed on the LLNL's High-Performance Computing Systems and were funded by the LLNL Computing Grand Challenge 16 "Broadband Earthquake Ground Motion Simulations on LLNL's Next Generation HPC Systems". The authors are grateful for Dr. Jeff Bayless's input toward completing the ground motion selection study.

10. References

Abrahamson, N. A., Silva, W. J., and Kamai, R. (2014). Summary of the ASK14 ground motion relation for active crustal regions. Earthquake Spectra, 30(3):1025–1055.

Ancheta, T. D., Darragh, R. B., Stewart, J. P., Seyhan, E., Silva, W. J., Chiou, B. S.-J., Wooddell, K. E., Graves, R. W., Kottke, A. R., Boore, D. M., et al. (2014). NGA-West2 database. Earthquake Spectra, 30(3):989–1005.

American Concrete Institute (2014). Building Code Requirements for Structural Concrete (ACI 318-14).

American Society of Civil Engineers (2017). Minimum Design Loads and Associated Criteria for Buildings and Other Structures (ASCE/SEI 7-16).

Baker, J.W. and Jayaram, N. (2008). Correlation of spectral acceleration values from NGA ground motion models. Earthquake Spectra, 24(1):299–317.

Boore, D. M. (2010). Orientation-independent, nongeometric-mean measures of seismic intensity from two horizontal components of motion. Bulletin of the Seismological Society of America, 100(4):1830–1835.

Boore, D. M., Stewart, J. P., Seyhan, E., and Atkinson, G. M. (2014). NGA-West2 equations for predicting PGA, PGV, and 5% damped PSA for shallow crustal earthquakes. Earthquake Spectra, 30(3):1057–1085.

Bradley, B. A. (2012). A ground motion selection algorithm based on the generalized conditional intensity measure approach. Soil Dynamics and Earthquake Engineering, 40:48–61.

Campbell, K. W. and Bozorgnia, Y. (2014). NGA-West2 ground motion model for the average horizontal components of PGA, PGV, and 5% damped linear acceleration response spectra. Earthquake Spectra, 30(3):1087–1115.

Chiou, B. S.-J. and Youngs, R. R. (2014). Update of the Chiou and Youngs NGA model for the average horizontal component of peak ground motion and response spectra. Earthquake Spectra, 30(3):1117–1153.

Giberson, M. F. (1967). The response of nonlinear multi-story structures subjected to earthquake excitation. PhD thesis, California Institute of Technology, Pasadena, CA.

Graves, R. and Pitarka, A. (2016). Kinematic ground-motion simulations on rough faults including effects of 3D stochastic velocity perturbations. Bulletin of the Seismological Society of America, 106(5):2136–2153.

Hayden, C. P., Bray, J. D., and Abrahamson, N. A. (2014). Selection of near-fault pulse motions. Journal of Geotechnical and Geoenvironmental Engineering, 140(7):04014030.

Ibarra, L. F., Medina, R. A., and Krawinkler, H. (2005). Hysteretic models that incorporate strength and stiffness deterioration. Earthquake engineering & structural dynamics, 34(12):1489–1511.

Kenawy, M. and McCallen, D. (2021). CCEER-20-07: Regional-scale seismic risk to reinforced concrete buildings based on physics-based earthquake ground motion simulations. Technical report, Center for Civil Engineering Earthquake Research, University of Nevada, Reno.

Kenawy, M., McCallen, D., and Pitarka, A. (2021). Variability of near-fault seismic risk to reinforced concrete buildings based on high-resolution physics-based ground motion simulations. Earthquake Engineering & Structural Dynamics, 50(6):1713–1733.

Kenawy, M. (2023). Ground motion selection for analysis of near-fault civil structures using broadband physics-based earthquake simulations. U.S. Geological Survey Final Technical Report.

Kenawy, M., McCallen, D., and Pitarka, A. (2023). Characteristics and selection of near-fault simulated earthquake ground motions for nonlinear analysis of buildings. Earthquake Spectra.

Luco, N. and Cornell, C. A. (2007). Structure-specific scalar intensity measures for near-source and ordinary earthquake ground motions. Earthquake Spectra, 23(2):357–392.

Marafi, N. A., Eberhard, M. O., Berman, J. W., Wirth, E. A., and Frankel, A. D. (2019). Impacts of simulated M9 Cascadia subduction zone motions on idealized systems. Earthquake Spectra, 35(3):1261–1287.

McCallen, D., Petersson, A., Rodgers, A., Pitarka, A., Miah, M., Petrone, F., Sjogreen, B., Abrahamson, N., and Tang, H. (2021a). EQSIM—a multidisciplinary framework for fault-to-structure earthquake simulations on exascale computers part I: Computational models and workflow. Earthquake Spectra, 37(2):707–735.

McKenna, F., Fenves, G. L., Scott, M. H., et al. (2000). Open system for earthquake engineering simulation. University of California, Berkeley, CA.

NEHRP Consultants Joint Venture (2011). Selecting and scaling earthquake ground motions for performing response-history analyses (NIST GCR 11-917-15). National Institute of Standards and Technology.

Pitarka, A., R. Graves, K. Irikura, K. Miyakoshi and A. Rodgers (2020). Kinematic rupture modeling of ground motion from the M7 Kumamoto, Japan earthquake. Pure and Applied Geophysics 177(5): 2199-2221.

Pitarka, A., R. Graves, K. Irikura, K. Miyakoshi, C. Wu, H. Kawase, A. Rodgers and D. McCallen (2022). Refinements to the Graves–Pitarka kinematic rupture generator, including a dynamically consistent slip rate function, applied to the 2019 Mw 7.1 Ridgecrest Earthquake. Bulletin of the Seismological Society of America 112(1): 287-306.

Shahi, S. K. and Baker, J. W. (2014a). An efficient algorithm to identify strong-velocity pulses in multicomponent ground motions. Bulletin of the Seismological Society of America, 104(5):2456–2466.

Shahi, S. K. and Baker, J.W. (2011). An empirically calibrated framework for including the effects of near-fault directivity in probabilistic seismic hazard analysis. Bulletin of the Seismological Society of America, 101(2):742–755.

Shahi, S. K. and Baker, J.W. (2014b). NGA-West2 models for ground motion directionality. Earthquake Spectra, 30(3):1285–1300.

Sjögreen, B., & Petersson, N. A. (2012). A fourth order accurate finite difference scheme for the elastic wave equation in second order formulation. Journal of Scientific Computing, 52, 17-48.

Somerville, P. G., Smith, N. F., Graves, R. W., and Abrahamson, N. A. (1997). Modification of empirical strong ground motion attenuation relations to include the amplitude and duration effects of rupture directivity. Seismological research letters, 68(1):199–222.

Tarbali, K. and Bradley, B. A. (2015). Ground motion selection for scenario ruptures using the generalised conditional intensity measure (GCIM) method. Earthquake Engineering & Structural Dynamics, 44(10):1601–1621.

Tarbali, K., Bradley, B. A., and Baker, J. W. (2019). Ground motion selection in the near-fault region considering directivity-induced pulse effects. Earthquake Spectra, 35(2):759–786.

Wang, G. (2011). A ground motion selection and modification method capturing response spectrum characteristics and variability of scenario earthquakes. Soil Dynamics and Earthquake Engineering, 31(4):611–625.

Zengin, E., & Abrahamson, N. A. (2021). A procedure for matching the near-fault ground motions based on spectral accelerations and instantaneous power. Earthquake Spectra, 37(4), 2545-2561.